Policy Research Journal
ISSN (E): 3006-7030 ISSN (P) : 3006-7022 Volume 4, Issue 3, 2026

EVALUATING CR_2O_3, G-C_3N_4 AND $TI_3C_2T_x$ MXENE NANOCOMPOSITES FOR VISIBLE-LIGHT-DRIVEN HYDROGEN PRODUCTION AND CO_2 REDUCTION

Rubina Qasim

Master of Philosophy in Chemistry, Forman Christian College (A Chartered University) Cum Laude, Pakistan

rubinaqasimb214@gmail.com

DOI: http://doi.org/10.5281/zenodo.24185944

Keywords
Photocatalysis; graphitic carbon nitride; chromium(III) oxide; $Ti_3C_2T_x$ MXene; hydrogen evolution; CO_2 reduction; heterojunction; visible light; nanocomposite.

Article History
Received: 12 January 2026
Accepted: 24 February 2026
Published: 11 March 2026

Copyright @Author
Corresponding Author: *
Rubina Qasim

Abstract
Efficient photocatalysts for renewable hydrogen production and carbon dioxide (CO_2) conversion are needed for sustainable energy technologies. Graphitic carbon nitride (g-C_3N_4) is a visible-light-responsive semiconductor, but rapid electron–hole recombination limits its activity. This proposed study evaluates a chromium(III) oxide/g-C_3N_4/$Ti_3C_2T_x$ ternary heterojunction for visible-light-driven hydrogen evolution and CO_2 reduction. Individual materials, binary composites, a physical-mixture control and ternary formulations will be compared under matched conditions. Characterisation will include XRD, Raman, FTIR, SEM/TEM-EDS, XPS, ICP-OES, BET, UV–Vis DRS, steady-state and time-resolved photoluminescence, photoelectrochemical and Mott–Schottky measurements. Hydrogen evolution rate, apparent quantum efficiency, CO_2 reduction product rates, electron-based selectivity (including competing H_2) and stability will be quantified, with product origin confirmed by $^{13}CO_2$ isotope labelling. Statistical analysis will use mean ± standard deviation, fold change, percentage improvement and Welch's ANOVA. Published g-C_3N_4/MXene data (Tables 1, 2, 4 and 5A) serve as benchmarks only and are not results for the proposed material.

1. Introduction

Rising energy demand, continued dependence on fossil fuels and growing atmospheric CO_2 have intensified interest in renewable energy technologies and carbon conversion. Hydrogen is a promising energy carrier because water is the principal product when it is used in fuel cells. Semiconductor photocatalysis, first demonstrated for water splitting at a TiO_2 electrode by Fujishima and Honda (1972), offers a route to convert solar energy into chemical energy. Photocatalytic CO_2 reduction similarly offers a way to convert captured carbon dioxide into useful products using light.

Photocatalysis involves light absorption, electron–hole pair generation, charge separation and surface redox reactions, and the efficiency of each step depends on the material's optical and electronic structure, interfaces and surface reaction sites (Kranz & Wächtler, 2021).

g-C_3N_4 has attracted attention because of its metal-free composition, visible-light response, chemical stability and accessible preparation. Wang et al. (2009) demonstrated hydrogen production from polymeric carbon nitride under

visible light. However, its efficiency is restricted by rapid charge-carrier recombination and limited active sites.

Two-dimensional MXenes are useful components of photocatalytic composites. $Ti_3C_2T_x$, obtained by selective removal of aluminium from Ti_3AlC_2 (Naguib et al., 2011), has a layered structure and surface terminations that influence interfacial charge transfer. Studies of g-C_3N_4/$Ti_3C_2T_x$ composites show that performance depends on composition and surface chemistry (Sun et al., 2018; Tambe et al., 2023).

Chromium(III) oxide (Cr_2O_3) is selected as the additional semiconductor component. Cr_2O_3 is a p-type semiconductor, so coupling with n-type g-C_3N_4 offers a plausible p–n heterojunction in which $Ti_3C_2T_x$ may act as an electron-collecting phase. This is a design hypothesis, not an established mechanism. The earlier working formula CrO has been replaced by Cr_2O_3 throughout, because CrO is not an established stable photocatalytic phase; the phase actually obtained must still be verified by XRD and XPS.

The study therefore investigates a Cr_2O_3/g-C_3N_4/$Ti_3C_2T_x$ ternary heterojunction for visible-light-driven hydrogen production and CO_2 reduction. Rather than assuming that three components improve activity, it compares individual components, binary composites, a physical mixture and ternary formulations under matched conditions.

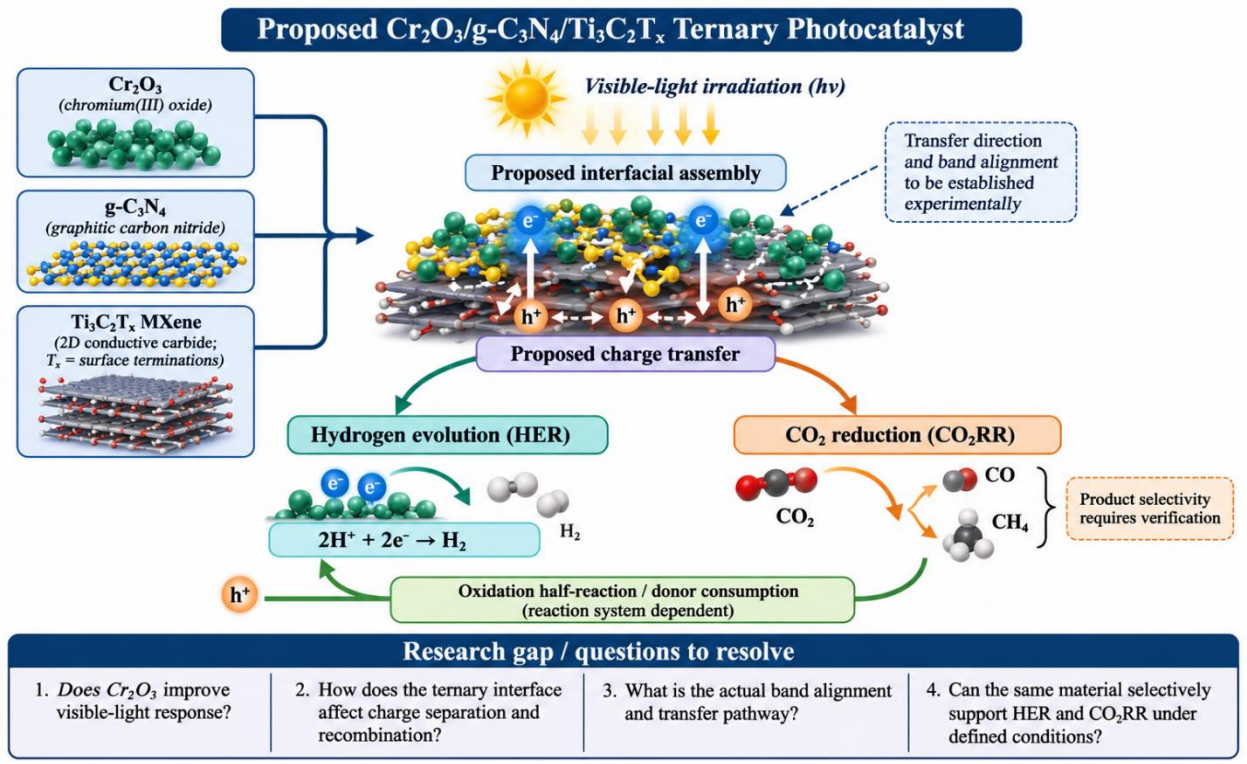


Figure 1. Conceptual representation of the proposed Cr_2O_3/g-C_3N_4/$Ti_3C_2T_x$ ternary photocatalyst and its potential applications in hydrogen evolution and CO_2 reduction.

2. Literature Review

2.1 g-C_3N_4 for photocatalytic hydrogen production

g-C_3N_4 is a polymeric semiconductor widely investigated for photocatalysis. Wang et al. (2009) provided the foundation for this field by demonstrating hydrogen production under visible light. Pristine g-C_3N_4 suffers from charge-carrier recombination and limited reaction efficiency, so structural modification, semiconductor coupling and cocatalyst incorporation have been explored. Their effectiveness depends on the resulting

electronic structure and interface quality; activity should therefore be reported together with structural, optical and electronic characterisation.

2.2 $Ti_3C_2T_x$ MXene and semiconductor heterojunctions

MXenes are two-dimensional transition-metal carbides and nitrides, of which $Ti_3C_2T_x$ is the most studied. Naguib et al. (2011) demonstrated its production by exfoliation of Ti_3AlC_2. In composites, $Ti_3C_2T_x$ may facilitate interfacial charge transfer and modify carrier behaviour.

Sun et al. (2018) studied a g-C_3N_4/$Ti_3C_2T_x$ composite with oxidised surface groups and reported 88 μmol g^{-1} h^{-1} of H_2, an apparent quantum yield of 1.27% and a 105% enhancement relative to their controls. Li et al. (2020) investigated a 2D/3D g-C_3N_4/Ti_3C_2 heterojunction for visible-light hydrogen evolution. Tambe et al. (2023) showed that hydrogen production varied substantially with the relative proportions of g-C_3N_4 and $Ti_3C_2T_x$, and Potapenko et al. (2025) reported improved hydrogen production for $Ti_3C_2T_x$-modified g-C_3N_4. Together these studies identify MXene content and surface chemistry as key variables.

2.3 Chromium(III) oxide as an additional semiconductor component

Cr_2O_3 is a p-type semiconductor with a visible-light-active band gap, and its coupling with g-C_3N_4 is a recognised heterojunction strategy. Its contribution cannot be assumed from its presence alone: phase, oxidation state, crystallinity and surface composition must be verified by XRD and XPS. Chromium-containing photocatalysts also raise a leaching and toxicity concern (Section 5.9). A systematic literature and patent search for Cr_2O_3/g-C_3N_4/MXene combinations must be completed before any novelty claim is made; this search is still outstanding.

2.4 Published quantitative evidence from related systems

Published studies supply benchmarks for choosing experimental variables. Sun et al. (2018) reported 88 μmol H_2 g^{-1} h^{-1} and an apparent quantum yield of 1.27%. Tambe et al. (2023) reported 1,912.25 μmol H_2 per 0.1 g for the best composition; the unit is retained because the irradiation time is needed to convert an accumulated amount to an hourly rate. Wong et al. (2024) reported 2,651.93 μmol g^{-1} h^{-1} with an apparent quantum efficiency of 7.26% at 420 nm for crystalline carbon nitride/MXene containing a Pt cocatalyst, 43.48 times higher than bare carbon nitride and 1.09 times higher than crystalline carbon nitride; this reflects the whole Pt-containing system and should not be attributed to MXene alone. For CO_2 reduction, Li et al. (2023) reported CO production eight times higher than g-C_3N_4 and twelve times higher than ZnO for a Ti_3C_2-decorated g-C_3N_4/ZnO photocatalyst.

Table 1. Published quantitative findings from related photocatalytic systems

Study	Reported result	Comparative finding	Relevance
Sun et al. (2018)	88 μmol H_2 g^{-1} h^{-1}	105% enhancement; AQY 1.27%	Influence of oxidised MXene surface groups
Wong et al. (2024)	2,651.93 μmol H_2 g^{-1} h^{-1}; AQE 7.26% (420 nm)	43.48-fold vs bare carbon nitride; 1.09-fold vs crystalline carbon nitride	Combined effect of crystallinity and Pt cocatalyst
Tambe et al. (2023)	1,912.25 μmol H_2 per 0.1 g	2.22 times the g-C_3N_4 value (860.98) and 25.5 times the $Ti_3C_2T_x$ value (74.90) from the same study	Composition-dependent hydrogen production
Li et al. (2023)	Improved CO production	8-fold vs g-C_3N_4; 12-fold vs ZnO	Potential improvement in CO_2 reduction

Composition-dependent findings of Tambe et al. (2023)

Table 2. Hydrogen generation reported for different g-C_3N_4/$Ti_3C_2T_x$ compositions

Catalyst formulation	Reported H_2 (µmol per 0.1 g)	Fold vs g-C_3N_4 (computed)
$Ti_3C_2T_x$	74.90	0.09
g-C_3N_4	860.98	1.00
gCT-1	1,410.21	1.64
gCT-0.75	1,912.25	2.22
gCT-0.50	1,296.23	1.51
gCT-0.25	1,150.32	1.34
gCT-0.05	1,021.23	1.19

These studies show that performance is sensitive to composition, surface modification and cocatalyst choice, which justifies systematic comparison rather than an assumed improvement.

3. Research Gap, Aim and Objectives

3.1 Research gap

g-C_3N_4, $Ti_3C_2T_x$ and their binary composites have been studied for hydrogen evolution, and MXene-containing semiconductor systems have been examined for CO_2 reduction (Table 1). What is missing is a controlled comparison of Cr_2O_3, g-C_3N_4 and $Ti_3C_2T_x$ within one experimental framework that tests (i) whether the ternary outperforms the best binary, (ii) whether a true heterojunction outperforms a physical mixture, and (iii) how composition links to charge-carrier behaviour in both hydrogen evolution and CO_2 reduction. The novelty of this exact composition must be confirmed by a systematic literature and patent search before it is claimed.

3.2 Research aim

To evaluate the structural, optical, electronic and photocatalytic properties of a Cr_2O_3/g-C_3N_4/$Ti_3C_2T_x$ ternary heterojunction for visible-light-driven hydrogen production and CO_2 reduction.

3.3 Research objectives

1. To prepare and characterise individual components and their binary, physical-mixture and ternary composites.
2. To investigate structural, morphological, optical and electronic properties.
3. To evaluate sacrificial hydrogen evolution under controlled visible-light irradiation.
4. To quantify CO_2 reduction products and confirm their carbon origin by $^{13}CO_2$ labelling.
5. To compare individual, binary and ternary formulations statistically.
6. To relate charge-carrier behaviour to photocatalytic activity.
7. To assess stability, activity retention and chromium leaching over repeated cycles.

3.4 Research questions

Q1 How does incorporating Cr_2O_3 and $Ti_3C_2T_x$ change the structural and optical properties of g-C_3N_4?

Q2 Does the ternary composite give a higher hydrogen evolution rate than its individual and binary components?

Q3 How does ternary composition affect CO_2 reduction product formation and electron-based selectivity?

Q4 How are charge-carrier lifetimes and photocurrent related to photocatalytic activity?

Q5 How stable is the composite, and does chromium leach during cycling?

3.5 Research hypotheses

Each hypothesis is stated so that it can be rejected by the data (alpha = 0.05, with multiplicity control). They are proposed for testing, not established findings.

H1: The H_2 evolution rate of the ternary composite (G7) is higher than that of the best binary composite (G4, G5 or G6).
H2: G7 gives a higher H_2 evolution rate than a physical mixture of the same overall composition (G7-PM), indicating a benefit from interfacial contact.
H3: H_2 evolution rate varies with the Cr_2O_3:$Ti_3C_2T_x$ mass ratio within the ternary series, with an optimum at an intermediate ratio.
H4: Across formulations, H_2 evolution rate is positively correlated with photocurrent density and with the photoluminescence lifetime-derived charge-carrier lifetime.
H5: G7 gives a higher ^{13}C-confirmed CO formation rate than G1 and G5.

4. Conceptual Framework

The framework links composition, interfacial structure, optical absorption, charge-carrier behaviour and reaction performance. g-C_3N_4 is the visible-light-responsive platform; Cr_2O_3 is a p-type partner whose contribution depends on its verified phase; $Ti_3C_2T_x$ may act as an electron-collecting phase that promotes charge separation and surface reactions.

The proposed pathway is a p–n junction at the Cr_2O_3/g-C_3N_4 interface with $Ti_3C_2T_x$ extracting electrons. This is a testable proposal only. Band-edge positions (Mott–Schottky, VB-XPS/UPS, DRS) and photoelectrochemical data will decide whether the observed behaviour is type-II, Z-scheme or Schottky-type, and none of these will be asserted beforehand. Hydrogen evolution proceeds through proton reduction by photogenerated electrons; CO_2 reduction proceeds through electron transfer to adsorbed CO_2 species, potentially giving CO or CH_4, with hydrogen evolution as a competing reaction.

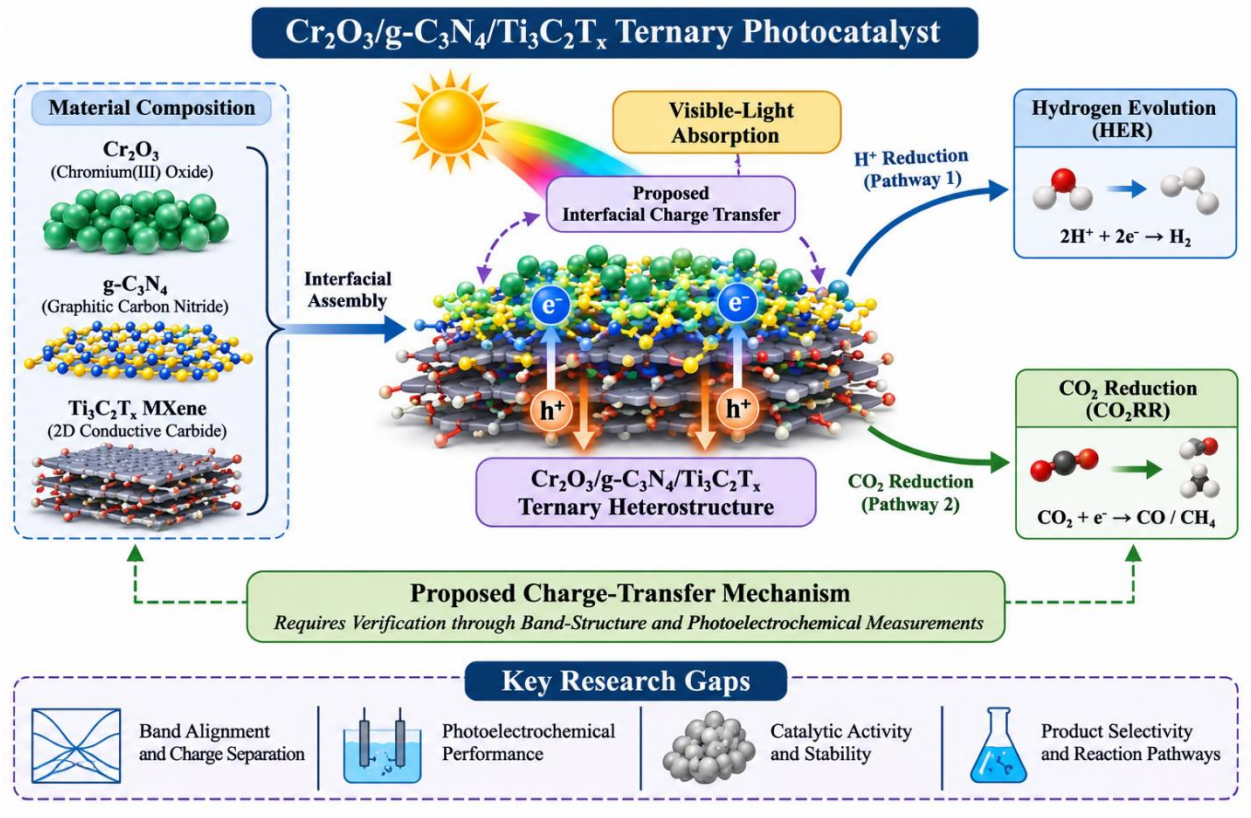


Figure 2. Conceptual relationship between ternary catalyst composition, interfacial charge transfer and photocatalytic reaction performance.

5. Materials and Methodology

5.1 Research design

A comparative experimental materials-science design used. Individual components, binary composites, a physical-mixture control and ternary formulations will be synthesised and tested under matched conditions, combining structural and optical characterisation with quantitative hydrogen and CO_2-reduction measurements.

5.2 Material preparation

g-C_3N_4 will be prepared by thermal condensation of a nitrogen-rich precursor (for example melamine or urea). $Ti_3C_2T_x$ will be prepared by selective etching and delamination of Ti_3AlC_2, or obtained from a verified supplier, and stored under inert conditions to limit oxidation to TiO_2. Cr_2O_3 will be prepared from a chromium(III) precursor such as chromium(III) nitrate nonahydrate, $Cr(NO_3)_3{\cdot}9H_2O$, followed by a controlled thermal treatment selected to give the Cr_2O_3 phase. The components will be combined by an in situ or electrostatic self-assembly route, and a physical mixture (G7-PM) of identical overall composition will be prepared by simple grinding or sonication.

Exact quantities, temperatures, times and solvent conditions will be fixed after phase confirmation and a pilot synthesis, and will be reported in full. Actual Cr loading will be measured by ICP-OES rather than assumed from the nominal ratio.

5.3 Experimental composition groups

Seven core groups plus one physical-mixture control will distinguish the effects of the individual materials, their combinations and interfacial contact.

Table 3. Proposed experimental composition groups

Group	Catalyst formulation	Experimental role
G1	g-C_3N_4	Semiconductor control
G2	Cr_2O_3	Chromium oxide control
G3	$Ti_3C_2T_x$	MXene control
G4	Cr_2O_3/g-C_3N_4	Binary heterojunction
G5	g-C_3N_4/$Ti_3C_2T_x$	Binary MXene composite
G6	Cr_2O_3/$Ti_3C_2T_x$	Binary control
G7	Cr_2O_3/g-C_3N_4/$Ti_3C_2T_x$	Proposed ternary composite
G7-PM	Physical mixture of Cr_2O_3, g-C_3N_4 and $Ti_3C_2T_x$ (same overall ratio as G7)	Tests the heterojunction versus a simple mixture

Additional ternary formulations will vary the Cr_2O_3 and MXene mass fractions; the series will be fixed after preliminary characterisation. All groups will be tested at matched catalyst loading, reaction volume, temperature, irradiation intensity and duration.

5.4 Structural and morphological characterisation

XRD will identify crystalline phases and confirm that the intended Cr_2O_3 phase and the structures of g-C_3N_4 and $Ti_3C_2T_x$ are retained. Raman and FTIR spectroscopy will confirm the integrity of g-C_3N_4 and the MXene. SEM and TEM with EDS mapping will examine morphology, layered structure, interfacial contact and elemental distribution. XPS will determine surface composition and oxidation states, with particular attention to Cr(III)/Cr(VI) and to Ti–O (oxidation) signals of the MXene. ICP-OES will determine actual Cr and Ti loading, and BET nitrogen sorption will give specific surface area and pore structure.

5.5 Optical and electronic characterisation

UV–Vis DRS will give absorption and estimated optical band gaps (Tauc analysis). Steady-state photoluminescence will be complemented by time-resolved photoluminescence, because PL intensity alone is not proof of improved charge separation. Photocurrent response and

electrochemical impedance spectroscopy will probe charge transport and interfacial resistance. Mott–Schottky analysis and VB-XPS or UPS will establish band-edge positions, and EPR will be used to detect radicals and defects, before any charge-transfer mechanism is assigned.

5.6 Photocatalytic hydrogen evolution

Experiments will use a sealed, top-irradiated reactor containing the catalyst dispersed in aqueous triethanolamine (TEOA) as sacrificial electron donor, irradiated by a 300 W Xe lamp with a $\lambda \geq 420$ nm cut-off filter. Irradiance will be measured with a calibrated radiometer, and the temperature held constant (for example 25 °C) by a circulating-water jacket, because dark MXene absorption can heat the suspension and inflate rates. These conditions are proposed and will be fixed in the final protocol. No noble-metal cocatalyst will be added to the main series so that the intrinsic ternary contribution is measured; a Pt-loaded benchmark may be run separately.

Because a sacrificial donor is used, the process will be called sacrificial photocatalytic hydrogen evolution, not overall water splitting. Overall water splitting will only be claimed if H_2 and O_2 are both detected in stoichiometric amounts. H_2 will be quantified by calibrated gas chromatography.

5.7 Photocatalytic CO_2 reduction

CO_2 reduction will be carried out in a sealed reactor under standardised catalyst loading, CO_2 supply, reaction medium and irradiation. Gaseous products (CO, CH_4 and H_2) will be quantified by calibrated GC, and liquid products, if formed, by suitable methods such as ion chromatography or NMR.

The following controls are mandatory: no catalyst, no light (dark), no CO_2, and an inert-gas (Ar instead of CO_2) run. Because g-C_3N_4 and residual organics can generate carbon-containing artefacts, isotope-labelled $^{13}CO_2$ experiments with GC–MS are mandatory, not optional, to confirm that CO and CH_4 originate from CO_2.

5.8 Stability assessment

Stability will be assessed over repeated cycles under identical conditions. Rates will be recorded each cycle, and the catalyst will be recharacterised after cycling (XRD, XPS, TEM) to detect structural or chemical change, including MXene oxidation to TiO_2. Activity retention and structural stability will be judged together.

5.9 Chromium leaching, safety and waste handling

After each cycling test the filtrate will be analysed for dissolved chromium by ICP-OES or ICP-MS, and for Cr(VI) by the diphenylcarbazide colorimetric method. Cr(VI) is toxic and carcinogenic, so all chromium-containing solids and solutions will be handled and disposed of as hazardous waste under institutional procedures, and any detected leaching will be reported with the stability results.

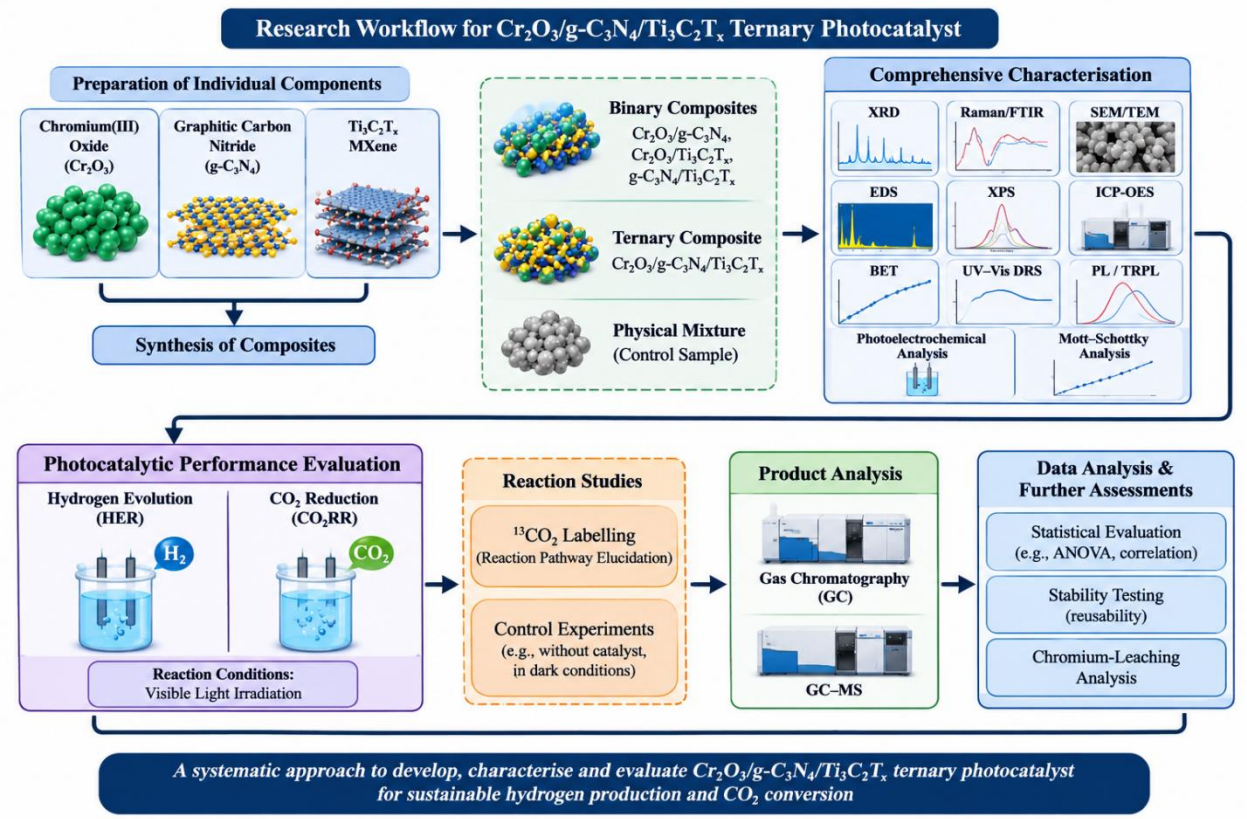


Figure 3. Proposed experimental synthesis, characterisation and photocatalytic testing workflow.

6. Photocatalytic Performance Calculations and Statistical Analysis

The equations below are proposed analytical procedures, not experimental results. They are inserted as native Word equations, so they remain editable and unchanged when the file is downloaded or opened elsewhere.

6.1 Hydrogen evolution rate

$$R_{H_2} = \frac{n_{H_2}}{m_{cat} \times t} \quad (1)$$

Where $R(H_2)$ is the hydrogen evolution rate (μmol g^{-1} h^{-1}), $n(H_2)$ the measured hydrogen amount (μmol), m(cat) the catalyst mass (g) and t the irradiation time (h).

6.2 Apparent quantum efficiency

$$AQE(\%) = \frac{2N_{H_2}}{N_{photons}} \times 100 \quad (2)$$

$N(H_2)$ is the number of H_2 molecules generated and N(photons) the number of incident photons; the factor of two reflects the two electrons required per H_2 molecule. The measurement wavelength and photon flux must be stated with every AQE value.

6.3 CO_2 reduction product formation rate

$$R_i = \frac{n_i}{m_{cat} \times t} \quad (3)$$

R(i) is the mass-normalised formation rate of product i (CO or CH_4) and n(i) the measured amount of that product.

6.4 Electron-based product selectivity

$$S_i(\%) = \frac{z_i n_i}{\sum_j z_j n_j} \times 100 \quad (4)$$

Here z(i) is the number of electrons consumed per molecule of product i (2 for H_2 and CO, 8 for CH_4). The sum runs over all reduction products including H_2, which competes with CO_2 reduction. Electron-based selectivity is used as the primary measure; the basis must always be stated, and molar fractions must not be interpreted as carbon- or electron-based selectivity.

6.5 Percentage improvement and fold change

$$I(\%)=\frac{R_{ternary}-R_{control}}{R_{control}}\times 100 \quad (5)$$

$$FC=\frac{R_{ternary}}{R_{control}} \quad (6)$$

Percentage improvement is undefined when the control rate is zero or below the detection limit; in that case the fold change is not defined either, and the detection limit is reported instead. Both are computed against controls tested under identical conditions, and the control used must always be named.

6.6 Mean and standard deviation

$$\bar{x}=\frac{\sum_{i=1}^{n} x_i}{n} \quad (7)$$

$$SD=\sqrt{\frac{\sum_{i=1}^{n}(x_i-\bar{x})^2}{n-1}} \quad (8)$$

Results are reported as mean ± sample standard deviation with the number of independent experiments, and individual data points are plotted alongside the summary statistics.

6.7 Percentage activity retention

$$A_{retention}(\%)=\frac{R_{final}}{R_{initial}}\times 100 \quad (9)$$

R(initial) is the first-cycle rate and R(final) the rate after the chosen number of cycles.

6.8 Analysis of variance

$$F=\frac{MS_{between}}{MS_{within}},\quad MS_{between}=\frac{SS_{between}}{k-1},\quad MS_{within}=\frac{SS_{within}}{N-k} \quad (10)$$

Here k is the number of groups and N the total number of observations. With only three independent runs per group, tests of normality and equal variance have very little power, so assumption checks cannot be relied on. Welch's ANOVA with Games–Howell post hoc comparisons will therefore be the default, with Tukey's test used only if variances are demonstrably similar and a non-parametric test if distributions are clearly non-normal. The sample size will be justified by a power analysis after a pilot run, and effect sizes (fold change with confidence intervals) will be reported alongside p-values, because statistical significance alone does not establish a meaningful improvement.

Table 4. Statistical indicators, reporting requirements and worked examples from previous studies

Indicator	Calculation	Unit / format	Purpose	Worked example from published data (not results of this study)
Hydrogen evolution rate	$n(H_2)$ / (m(cat) × t)	μmol g^{-1} h^{-1}	Compare H_2 production	Reported: Sun et al. 88; Wong et al. 2,651.93 μmol g^{-1} h^{-1}. Tambe et al.: 1,912.25 μmol per 0.1 g, i.e. 19,122.5 μmol g^{-1} accumulated; no hourly rate can be derived because the irradiation time is not in the compiled data.
Apparent quantum efficiency	$2N(H_2)$ / N(photons) × 100	% (state λ)	Photon utilisation	Reported: Sun et al. 1.27%; Tambe et al. (gCT-0.75) 3.1%; Wong et al. 7.26% at 420 nm.
CO formation rate	n(CO) / (m(cat) × t)	μmol g^{-1} h^{-1}	Quantify CO production	Li et al. (2023): CO production 8× that of g-C_3N_4 and 12× that of ZnO. Absolute rates are not in the compiled data.
Electron-based selectivity	z(i)n(i) / Σ z(j)n(j) × 100 (H_2 included)	%	Product distribution	Not available in the compiled sources; to be measured in this study.
Percentage improvement	(R(ter) − R(ctrl)) / R(ctrl) × 100	%	Compare formulations	Reported: Sun et al. 105%. Computed from Tambe et al.: gCT-0.75 vs g-C_3N_4 = 122.1%; vs $Ti_3C_2T_x$ = 2,453%. Wong et al.: 43.48-fold vs bare carbon nitride =

				4,248%. Li et al.: 8-fold = 700%; 12-fold = 1,100%.
Fold change	R(ter) / R(ctrl)	× (state control)	Comparison when control ≈ 0	Computed from Tambe et al.: gCT-0.75 is 2.22× g-C_3N_4 and 25.5× $Ti_3C_2T_x$.
Mean	Arithmetic average	Data unit	Central tendency	Tambe et al., five g-C_3N_4/$Ti_3C_2T_x$ compositions (Table 2): mean = 1,358.05 µmol per 0.1 g. This averages different compositions, not replicates.
Standard deviation	Sample SD (n − 1)	Data unit	Experimental variability	Same five compositions: SD = 342.88 µmol per 0.1 g. This is spread between compositions, not replicate variability; replicate SDs were not available in the compiled data.
Activity retention	R(final) / R(initial) × 100	%	Catalyst stability	Not reported in the compiled sources; to be measured in this study.
ANOVA	F = MS(between) / MS(within); Welch's ANOVA default	F, p	Test group differences	Not applicable to the published values, which are single reported values without replicate data; requires replicate runs from this study.

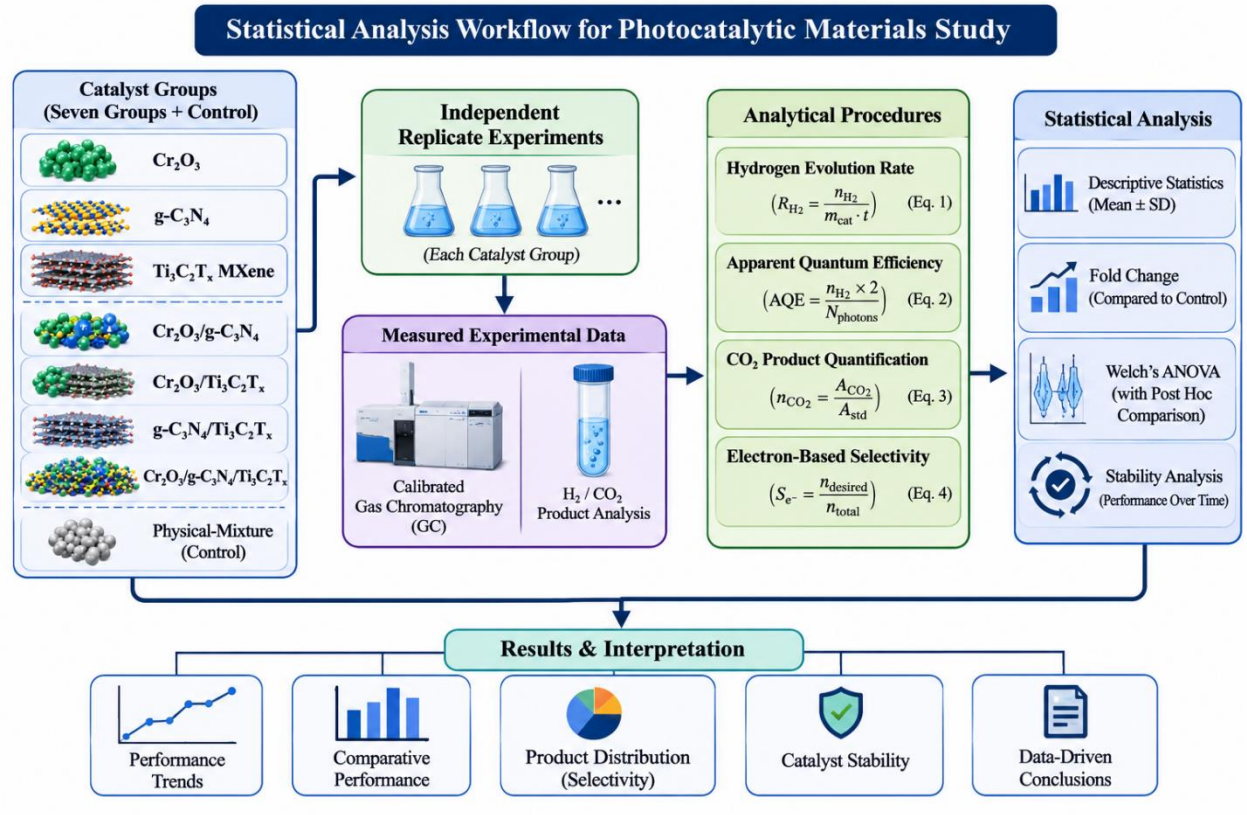


Figure 4. Proposed statistical workflow for comparing photocatalytic performance.

7. Experimental Data Collection and Reference Data

Table 5A collects the quantitative data from previous studies, mapped to the closest proposed group, so that future measurements can be benchmarked directly. Table 5B is the data-recording template for this study. Values in 5A are published results from other materials; the fields in 5B are empty until experiments are performed.

Table 5A. Reference data from previous studies mapped to the proposed groups (published values; not results of this study)

Study and system	H_2 reported	Comparative result	Closest proposed group
Sun et al. (2018): g-C_3N_4/$Ti_3C_2T_x$, oxidised surface groups	88 μmol g^{-1} h^{-1}	105% enhancement vs controls	G5
Tambe et al. (2023): gCT-0.75	1,912.25 μmol per 0.1 g	2.22× g-C_3N_4; 25.5× $Ti_3C_2T_x$	G5
Tambe et al. (2023): g-C_3N_4	860.98 μmol per 0.1 g	Reference control in that study	G1
Tambe et al. (2023): $Ti_3C_2T_x$	74.90 μmol per 0.1 g	Reference control in that study	G3
Wong et al. (2024): crystalline carbon nitride/$Ti_3C_2T_x$ with Pt	2,651.93 μmol g^{-1} h^{-1}	43.48× bare carbon nitride; 1.09× crystalline carbon nitride	G5-type; Pt-containing, not directly comparable

IER
Institute for Excellence in Education & Research

8. Planned Interpretation

Structural and optical data will show whether composite formation changes phase composition, absorption and carrier lifetimes; no single technique (PL, DRS or XPS) will be treated as proof of a charge-transfer mechanism. For hydrogen evolution, the benchmark values in Table 5A show that g-C_3N_4/MXene systems can reach different performances depending on composition, surface chemistry and cocatalyst, but they are not predictions for the Cr_2O_3-containing material. Comparison of G7 with G4, G5, G6 and G7-PM will show whether any gain comes from the combined interface rather than one active component.

For CO_2 reduction, rates and electron-based selectivity (with H_2 counted) will be interpreted only after control experiments and $^{13}CO_2$ labelling confirm product origin. Effect size, variability and reproducibility will be weighed together with significance tests, and a high initial rate with rapid decay or chromium leaching will be judged to have limited practical value.

9. Research Implications

The study may clarify how interfaces influence optical response and charge-carrier behaviour in multi-component photocatalysts, provide evidence on the potential of the material for solar hydrogen production, and show whether the composite can contribute to photocatalytic carbon conversion. Any claim about practical carbon utilisation depends on verified product formation, selectivity and efficiency. The results may also guide later optimisation of component ratios, surface modification, cocatalysts and reaction conditions.

10. Limitations

1. The Cr_2O_3 phase is the intended one but has not yet been confirmed experimentally.
2. The material has not yet been synthesised, so no original rates, quantum efficiencies, significance values or stability data exist.
3. Results depend on irradiation intensity, photon flux, loading, temperature, pH, sacrificial reagent and reactor design, which must be controlled and reported.
4. The ternary composite may not outperform its binary components; this is the question being tested.
5. CO_2 reduction products need careful verification because background carbon can mimic products.
6. Laboratory performance does not demonstrate commercial feasibility; scalability, long-term stability, cost, chromium toxicity and environmental impact require further study.
7. Benchmark values come from different published experiments and conditions and cannot be pooled or treated as predictions.

11. Conclusion

This proposed study will compare a Cr_2O_3/g-C_3N_4/$Ti_3C_2T_x$ MXene ternary heterojunction with its individual components, binary composites and a physical mixture for visible-light-driven hydrogen production and CO_2 reduction. The methodology combines synthesis, extended structural, optical and electronic characterisation, sacrificial hydrogen evolution, isotope-verified CO_2 reduction, chromium-leaching analysis and statistical analysis suited to small replicate numbers. Published g-C_3N_4/MXene data (Tables 1, 2, 4 and 5A) provide benchmarks but cannot be transferred to the chromium-containing composite, whose performance, mechanism and stability must be established experimentally.

REFERENCES

Fujishima, A., & Honda, K. (1972). Electrochemical photolysis of water at a semiconductor electrode. *Nature, 238*, 37–38. https://doi.org/10.1038/238037a0

Kranz, C., & Wächtler, M. (2021). Characterizing photocatalysts for water splitting: From atoms to bulk and from slow to ultrafast processes. *Chemical Society Reviews, 50*(2), 1407–1437. https://doi.org/10.1039/D0CS00526F

Li, J., Zhao, L., Wang, S., Li, J., Wang, G., & Wang, J. (2020). In situ fabrication of 2D/3D g-C_3N_4/Ti_3C_2 (MXene) heterojunction for efficient visible-light photocatalytic hydrogen evolution. *Applied Surface Science, 515*, Article 145922. https://doi.org/10.1016/j.apsusc.2020.145922

Li, J., Wang, Y., Wang, Y., Guo, Y., Zhang, S., Song, H., Li, X., Gao, Q., Shang, W., Hu, S., Zheng, H., & Li, X. (2023). MXene Ti_3C_2 decorated g-C_3N_4/ZnO photocatalysts with improved photocatalytic performance for CO_2 reduction. *Nano Materials Science, 5*(2), 237–245. https://doi.org/10.1016/j.nanoms.2023.02.003

Naguib, M., Kurtoglu, M., Presser, V., Lu, J., Niu, J., Heon, M., Hultman, L., Gogotsi, Y., & Barsoum, M. W. (2011). Two-dimensional nanocrystals produced by exfoliation of Ti_3AlC_2. *Advanced Materials, 23*(37), 4248–4253. https://doi.org/10.1002/adma.201102306

Potapenko, K. O., Vasilchenko, D. B., Kurenkova, A. Y., Saraev, A. A., Mishchenko, D. D., Gerasimov, E. Y., & Kozlova, E. A. (2025). Expanding g-C_3N_4 capabilities for photocatalytic H_2 production by modification with $Ti_3C_2T_x$ MXene. *International Journal of Hydrogen Energy, 99*, 291–300. https://doi.org/10.1016/j.ijhydene.2024.12.213

Sun, Y., Jin, D., Sun, Y., Meng, X., Gao, Y., Dall'Agnese, Y., Chen, G., & Wang, X.-F. (2018). g-C_3N_4/$Ti_3C_2T_x$ (MXenes) composite with oxidized surface groups for efficient photocatalytic hydrogen evolution. *Journal of Materials Chemistry A, 6*(19), 9124–9131. https://doi.org/10.1039/C8TA02706D

Tambe, A. B., Arbuj, S. S., Umarji, G. G., Kulkarni, S. K., & Kale, B. B. (2023). In situ synthesis of g-C_3N_4/$Ti_3C_2T_x$ nano-heterostructures for enhanced photocatalytic H_2 generation via water splitting. *RSC Advances, 13*(50), 35369–35378. https://doi.org/10.1039/D3RA07321A

Wang, X., Maeda, K., Thomas, A., Takanabe, K., Xin, G., Carlsson, J. M., Domen, K., & Antonietti, M. (2009). A metal-free polymeric photocatalyst for hydrogen production from water under visible light. *Nature Materials, 8*(1), 76–80. https://doi.org/10.1038/nmat2317

Wong, K. J., Foo, J. J., Siang, T. J., Khoo, V., & Ong, W.-J. (2024). Harnessing the power of light: The synergistic effects of crystalline carbon nitride and $Ti_3C_2T_x$ MXene in photocatalytic hydrogen production. *Global Challenges, 8*(6), Article 2300235. https://doi.org/10.1002/gch2.202300235

IEER
Institute for Excellence in Education & Research